Porous Media Based Modeling of parallel Plate PE-CVD Apparatus: Approximation to the Experiments with SiC and TiC.

J.GEISER[1] and M.ARAB[2]

[1]*Humboldt-Universität zu Berlin,Department of Mathematics, Unter den Linden 6, D-10099*

Berlin, Germany

Email: geiser@mathematik.hu-berlin.de

[2]*Humboldt-Universität zu Berlin,Department of Mathematics, Unter den Linden 6, D-10099*

Berlin, Germany

Email: arab@mathematik.hu-berlin.de

ABSTRACT

The numerous technical applications in deposit metal plates with new materials like SiC and TiC has an advantage to overcome the leaking corrosive behavior and have additional a good electrical behavior. Here we present an application of a porous media to model a homogenized deposition with a parallel plate PE-CVD apparatus. Special geometries of parallel Anodes and cathodes helps to obtain at least a laminar flow field. By the way the delicate arrangement of the anode and cathode has to be simulated. The flux of the precursors are important to simulate to the porous media given as the plasma background. Here we can optimize the transport to the delicate geometry respecting the flux field in the permeable layers. To derive a mathematical model, we deal with a model for the transport and kinetics of the different species. Underlying physical experiments help to approximate the parameters of the numerical model. We introduce a multi regression method to approximate the physical to the mathematical parameters. We present results of some numerical simulations and help to foresee some effects to find on optimal deposition process.

Keywords: numerical methods, CVD processes, regression method, iteration process, opti-

mization.

AMS subject classifications. 35K25, 35K20, 74S10, 70G65.

1 INTRODUCTION

We motivate our studying on simulating a thin film deposition process that can be done with plasma enhanced chemical vapor deposition (PECVD) processes. In the last years, due to the research in producing high temperature films by depositing of low pressure, processes have increased. The interest on standard applications to SiC and TiC are immense but delicate to model and optimize a homogene deposition rate, which is important to achieve a stable nanolayer.

We present a model for the transport and kinetic processes of the precursor gases in a low temperature and low pressure plasma. We take into account the transport and kinetics of CVD processes in the reactor and the retardation of molecules, which are treated by the underlying process plasma.

The model is discussed as a transport-reaction model with systems of coupled partial and ordinary differential equations.

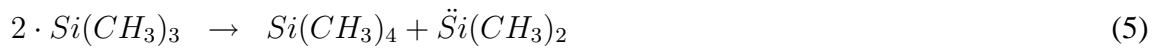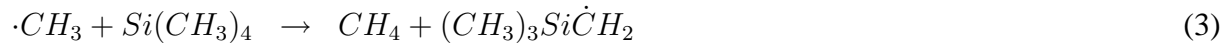The paper is outlined as follows.

In section 2 and 3 we present the physical and mathematical model and a possible reduced model for the further approximations. In section 4 we present the underlying discretization methods and analysis of the coupled model equations. The approximation to the physical parameters are discussed in Section 5. The numerical experiments are given in Section 6. In the contents, that is given in Section 7, we summarize our results.

2 PHYSICAL MODEL AND EXPERIMENTS TO SIC AND TIC

The base of the experimental setup is the plasma reactor chamber of a NIST *GEC reference cell*. The spiral antenna of a hybrid ICP/CCP-RF plasma source was replaced by a double spiral antenna (Kadetov 2004). This reduces the asymmetry of the magnetic field due to the superposition of the induced fields of both antennas. Also, the power coupling to the plasma increases and
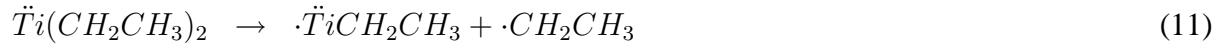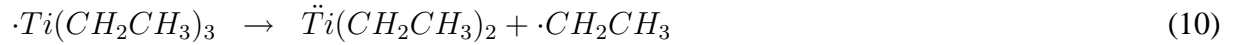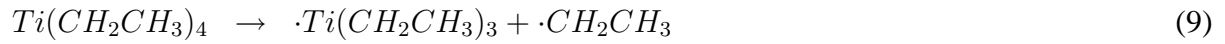
enhances the efficiency of the source. A set of MKS mass flow-controllers allow any defined mixture of gaseous precursors. Even the flows of liquid precursors with high vapor pressure is controlled by this system. All other liquid and all solid precursors will be directly transported to the chamber by a controlled carrier gas flow. Besides the precursor flow, the density can also be changed by varying the pressure inside the recipient. Controlling the pressure is achieved with a valve between the recipient and vacuum pumps. In addition, a heated and insulated substrate holder was mounted. Thus, a temperature up to 800^oC and a bias voltage can be applied to the substrate. While the pressure and RF power determine the undirected particle energy (plasma temperature), the bias voltage adds, only to the charged particles, energy directed at the substrate. Apart from the pressure and RF power control, the degree of ionization and number as well as size of molecular fractions can be controlled.

For the precursor of SiC is given via Tetramethyl-silane and have the following reaction mechanism:

$$Si(CH_3)_4 \quad \rightarrow \quad \cdot CH_3 + \cdot Si(CH_3)_3 \tag{1}$$

$$\cdot CH_3 + H_2 \quad \rightarrow \quad CH_4 + \cdot H \tag{2}$$

$$\cdot CH_3 + Si(CH_3)_4 \quad \rightarrow \quad CH_4 + (CH_3)_3 Si\dot{C}H_2 \tag{3}$$

$$\cdot Si(CH_3)_3 + H_2 \quad \rightarrow \quad HSi(CH_3)_3 + \dot{H} \tag{4}$$

$$2 \cdot Si(CH_3)_3 \quad \rightarrow \quad Si(CH_3)_4 + \ddot{S}i(CH_3)_2 \tag{5}$$

$$Si(CH_3)_4 + H_2 \quad \rightarrow \quad HSi(CH_3)_3 + CH_4 \tag{6}$$

$$HSi(CH_3)_3 \quad \rightarrow \quad \ddot{S}i(CH_3)_2 + CH_4 \tag{7}$$

$$\ddot{S}i(CH_3)_2 \quad \rightarrow \quad \dot{S}iH_2\dot{C}H_2 \tag{8}$$

The last reaction ends up in the deposition of SiC.

For the precursor of TiC is given via Tetraethyl-titanium and we have the following kinetics:

$$Ti(CH_2CH_3)_4 \quad \rightarrow \quad \cdot Ti(CH_2CH_3)_3 + \cdot CH_2CH_3 \tag{9}$$

$$\cdot Ti(CH_2CH_3)_3 \quad \rightarrow \quad \ddot{T}i(CH_2CH_3)_2 + \cdot CH_2CH_3 \tag{10}$$

$$\ddot{T}i(CH_2CH_3)_2 \quad \rightarrow \quad \cdot \dddot{T}iCH_2CH_3 + \cdot CH_2CH_3 \tag{11}$$

Additionally we can use a titanium precursor shown in Figure 1. Here we can step by step separate the $\cdot CH_3$ groups.
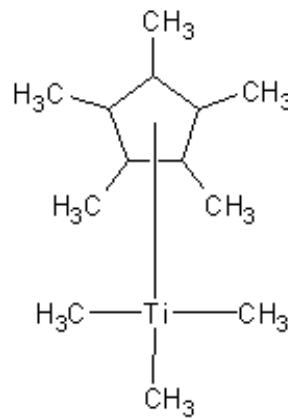

Figure 1: Cp*TiMe3 or (Trimethyl)pentamethylcyclopentadienyltitanium(IV)

3   MATHEMATICAL MODEL

In the following the models are discussed in two directions of far-field and near-field problems:

1. Reaction-diffusion equations, see (Gobbert and Ringhofer 1998) (far-field problems);

2. Boltzmann-Lattice equations, see (Senega and Brinkmann 2006) (near-field problems).

3. Reaction equations, see (Geiser and Arab 2008) (kinetic problems).

The modeling of the far- and near-field problems are considered by the Knudsen number (Kn) which is the ratio of the mean free path λ over the typical domain size L. For small Knudsen numbers $Kn \approx 0.01 - 1.0$ we apply the convection-diffusion equation, whereas for large

4

Knudsen numbers $Kn \geq 1.0$ we deal with a Boltzmann equation, see (Ohring 2002). For the kinetic problems we only consider the chemical reaction between the species, see (Geiser and Arab 2008).

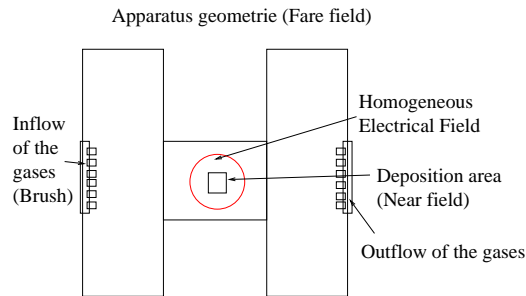The geometry of fare field apparatus is given as:

Apparatus geometrie (Fare field)

Figure 2: Fare field of the parallel PECVD apparatus.

The geometry of the near field apparatus is given as:

Apparatus geometrie (Near field)

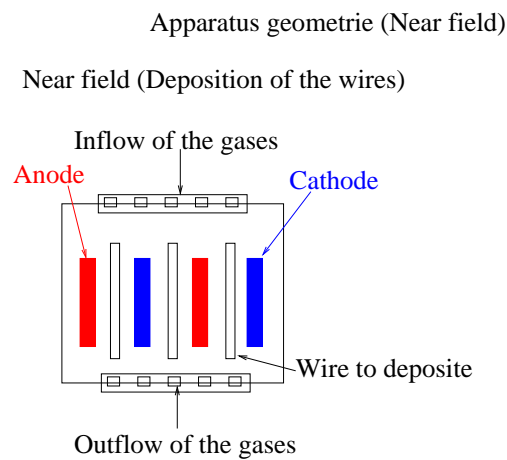Near field (Deposition of the wires)

Figure 3: near field of the deposition area.

3.1 Model for Small Knudsen Numbers (Far-field Model)

When gas transport is physically more complex due to combined flows in three dimensions, the fundamental equations of fluid dynamics become the starting point of the analysis. For our models with small Knudsen numbers we can assume a continuum flow. The fluid equations can be treated with a Navier-Stokes or especially with a convection-diffusion equation.

5

Three basic equations describe the conservation of mass, momentum and energy that are sufficient to describe the gas transport in the reactors, see (Ohring 2002).

1. Continuity - the conservation of mass requires the net rate of mass accumulation in a region to be equal to the difference between the inflow and outflow rates.

2. Navier-Stokes - momentum conservation requires the net rate of momentum accumulation in a region to be equal to the difference between the in- and out-rate of the momentum, plus the sum of the forces acting on the system.

3. Energy - the rate of accumulation of internal and kinetic energy in a region is equal to the net rate of internal and kinetic energy by convection, plus the net rate of heat flow by conduction, minus the rate of work done by the fluid.

We will concentrate on the conservation of mass and assume that energy and momentum are conserved, see (Gobbert and Ringhofer 1998) and (Geiser 2001). Therefore the continuum flow can be described as a convection-diffusion equation given as:

$$\phi \partial_t c_i + \nabla \cdot (\mathbf{v} c_i - D^{e(i)} \nabla c_i) = -\lambda_i \phi c_i + \sum_{k=k(i)} \lambda_k \phi c_k + \tilde{Q}_i, \tag{12}$$

where we have the following parameters

$\phi :$ effective porosity $[-]$,

$c_i :$ concentration of the ith species, e.g. Si, Ti, C

      phase $[mol/mm^3]$,

$\mathbf{v} :$ Velocity in the underlying plasma atmosphere $[mm/s]$,

$D^{e(i)} :$ element specific diffusions-dispersions tensor $[mm^2/s]$,

$\lambda_i :$ decay constant of the ith species $[1/s]$,

$\tilde{Q}_i :$ source term of the ith species $[mol/(m^3 s)]$,

with $i = 1, \ldots, M$ and M denotes the number of species.

The effective porosity is denoted by ϕ and declares the portion of the porosities of the aquifer (air), that is filled with the ionized plasma. The transport term is indicated by the velocity $\mathbf{v}$, that presents the direction and the absolute value of the plasma flux in the apparatus. The velocity field is divergence-free. The kinetic constant of the ith species is denoted by λ_i. Thereby does $k(i)$ denote the indices of the successor species. The initial value is given as $c_{i,0}$ and we assume a Dirichlet boundary with the function $c_{i,1}(x, t)$ sufficiently smooth.

3.2 Model for Large Knudsen Numbers (Near-field Model)

The model assumes that the heavy particles can be described with a dynamical fluid model, where the elastic collisions define the dynamics and few inelastic collisions are, among other reasons, responsible for the chemical reactions.

To describe the individual mass densities as well as the global momentum and the global energy as dynamic conservation quantities of the system corresponding conservation equations are derived from Boltzmann equations.

The individual character of each species is considered by mass-conservation equations and the so-called difference equations.

The Boltzmann equation for heavy particles (ions and neutral elements) is given as:

$$\frac{\partial}{\partial t} n_s + \frac{\partial}{\partial \boldsymbol{r}} \cdot (n_s \boldsymbol{u} + n_s c_s) = Q_n^{(s)}, \tag{13}$$

$$\frac{\partial}{\partial t} \rho \boldsymbol{u} + \frac{\partial}{\partial \boldsymbol{r}} \cdot \left(\rho \boldsymbol{u} \boldsymbol{u} + nT\underline{\underline{I}} - \underline{\underline{\tau}}^* \right) = \sum_{s=1}^{N} q_s n_s \langle \boldsymbol{E} \rangle, \tag{14}$$

$$\frac{\partial}{\partial t} \mathcal{E}_{\text{tot}}^* + \frac{\partial}{\partial \boldsymbol{r}} \cdot \left(\mathcal{E}_{\text{tot}}^* \boldsymbol{u} + \boldsymbol{q}^* + nT\boldsymbol{u} - \underline{\underline{\tau}}^* \cdot \boldsymbol{u} \right)$$
$$= \sum_{s=1}^{N} q_s n_s \left(\boldsymbol{u} + \boldsymbol{c}_s \right) \cdot \langle \boldsymbol{E} \rangle - Q_{\mathcal{E},\text{inel}}^{(e)}, \tag{15}$$

where ρ denotes the mass density, $\boldsymbol{u}$ is the velocity, and T the temperature of the ions. $\mathcal{E}_{\text{tot}}^*$ is the

total energy of the heavy particles; n_s is the particle density of heavy particles species s; $\boldsymbol{q}^*$ is the heat flux of the heavy particle system; $\underline{\underline{\tau}}^*$ is the viscous stress of the heavy particle system; $\boldsymbol{E}$ is the electric field and $Q_{\mathcal{E}}$ is the energy conservation.

Further, the production terms are $Q_n^{(s)} = \sum_r a_{\text{sign}} k_{\alpha,r} n_\alpha n_r$ with rate coefficients $k_{\alpha,r}$.

We have drift diffusion for heavy particles in the following fluxes. The dissipative fluxes of the impulse and energy balance are linear combinations of generalized forces:

$$\boldsymbol{q}^* = \lambda_E \langle \boldsymbol{E} \rangle - \lambda \frac{\partial}{\partial \boldsymbol{r}} T - \sum_{s=1}^{N} \sum_{\alpha=1}^{N} \lambda_n^{(\alpha,s)} \frac{1}{n_s} \frac{\partial}{\partial \boldsymbol{r}} n_\alpha, \tag{16}$$

$$\underline{\underline{\tau}}^* = -\eta \left(\frac{\partial}{\partial \boldsymbol{r}} \boldsymbol{u} + \left(\frac{\partial}{\partial \boldsymbol{r}} \boldsymbol{u} \right)^\top - \frac{2}{3} \left(\frac{\partial}{\partial \boldsymbol{r}} \cdot \boldsymbol{u} \right) \underline{\underline{I}} \right), \tag{17}$$

$$\mathcal{E}_{\text{tot}}^* = \sum_{s=1}^{N} 1/2 \rho_s c_s^2 + 1/2 \rho u^2 + 3/2 n T. \tag{18}$$

where λ is the thermal diffusion transport coefficient. T is the temperature, n is the particle density.

Diffusions of the species are underlying to the given plasma and are described by the following equations:

$$\frac{\partial}{\partial t} n_s + \frac{\partial}{\partial \boldsymbol{r}} \cdot (n_s \boldsymbol{u} + n_s \boldsymbol{c}_s) = Q_n^{(s)}, \tag{19}$$

$$\boldsymbol{c}_s = \mu_s \langle \boldsymbol{E} \rangle - d_T^{(s)} \frac{\partial}{\partial \boldsymbol{r}} T - \sum_{\alpha=1}^{N} D_n^{(\alpha,s)} \frac{1}{n_s} \frac{\partial}{\partial \boldsymbol{r}} n_\alpha. \tag{20}$$

The density of the species is of dynamical values and the species' transport and mass transport are subject to the following constraint conditions:

$$\sum_s m_s n_s = \rho, \tag{21}$$

$$\sum_s n_s m_s \boldsymbol{c}_s = 0. \tag{22}$$

where m_s is the mass of the heavy particle, n_s is the density of the heavy particle, and c_s is the difference-velocity of the heavy particle.

Field Model

The plasma transport equations are Maxwell equations and are coupled with a field. They are given as:

$$\frac{1}{\mu_0}\nabla \times \boldsymbol{B}_{\text{dyn}} = -en_e\boldsymbol{u}_e + \tilde{\boldsymbol{j}}_{\text{ext}}, \tag{23}$$

$$\nabla \cdot \boldsymbol{B}_{\text{dyn}} = 0, \tag{24}$$

$$\nabla \times \boldsymbol{E} = -\frac{\partial}{\partial t}\boldsymbol{B}_{\text{dyn}}, \tag{25}$$

where $\boldsymbol{B}$ is the magnetic field and $\boldsymbol{E}$ is the electric field.

3.3 Simplified Model for Large Knudsen Numbers (Near-field Model)

For the numerical analysis and for the computational results, we reduce the complex model and derive a system of coupled Boltzmann and diffusion equations.

We need the following assumptions:

$$\boldsymbol{q}^* = -\lambda\frac{\partial}{\partial \boldsymbol{r}}T, \tag{26}$$

$$\underline{\underline{\tau}}^* = 0, \tag{27}$$

$$\mathcal{E}_{\text{tot}}^* = 3/2nT, \tag{28}$$

$$Q_{\mathcal{E},\text{inel}}^{(e)} = \text{const}, \tag{29}$$

and obtain a system of equations:

$$\frac{\partial}{\partial t}\rho + \frac{\partial}{\partial \boldsymbol{r}} \cdot (\rho \boldsymbol{u}) = 0, \tag{30}$$

$$\frac{\partial}{\partial t}\rho \boldsymbol{u} + \frac{\partial}{\partial \boldsymbol{r}} \cdot \left(\rho \boldsymbol{u}\boldsymbol{u} + nT\underline{\underline{I}}\right) = \sum_{s=1}^{N} q_s n_s \langle \boldsymbol{E} \rangle, \tag{31}$$

$$\frac{\partial}{\partial t}3/2nT + \frac{\partial}{\partial \boldsymbol{r}} \cdot \left(3/2nT\boldsymbol{u} + \lambda\frac{\partial}{\partial \boldsymbol{r}}T + nT\boldsymbol{u}\right)$$

$$= \sum_{s=1}^{N} q_s n_s \left(\boldsymbol{u} + \boldsymbol{c}_s\right) \cdot \langle \boldsymbol{E} \rangle - Q_{\mathcal{E},\mathrm{inel}}^{(e)} . \tag{32}$$

Remark 1 *We obtain three coupled equations for density, velocity and temperature of the plasma. The equations are strong-coupled and decomposition can be done in discretized form.*

4 NUMERICAL METHODS: DISCRETIZATION OF THE CONVECTION-DIFFUSION EQUATION

For the space-discretization we use finite-volume methods and for the time-discretization we apply explicit or implicit Euler methods. In the next sections we introduce the notation for the space-discretization and describe the discretization-methods for each equation-part.

4.1 Notation

The time-steps for the calculation in the time-intervals are $(t^n, t^{n+1}) \subset (0, T)$, for $n = 0, 1, \dots$. The computational cells are given as $\Omega_j \subset \Omega$ with $j = 1, \dots, I$. The unknown I is the number of the nodes.

For the application of finite-volumes we have to construct a dual mesh for the triangulation $\mathcal{T}$, for the domain Ω. First the finite-elements for the domain Ω are given by $T^e, e = 1, \dots, E$. The polygonal computational cells Ω_j are related to the vertices x_j of the triangulation.

The notation for the relation between the neighbor cells and the concerned volume of each cell is given in the following notation.

Let $V_j = |\Omega_j|$ and the set Λ_j denote the neighbor-point x_k to the point x_j. The boundary of the

10

cell j and k is denoted as Γ_{jk}.

We define the flux over the boundary Γ_{jk} as

$$v_{jk} = \int_{\Gamma_{jk}} \mathbf{n} \cdot \mathbf{v} \, ds \, . \tag{33}$$

The inflow-flux is given as $v_{jk} < 0$, and the outflow-flux is $v_{jk} > 0$. The antisymmetry of the fluxes is denoted as $v_{jk} = -v_{kj}$. The total outflow-flux is given as

$$\nu_j = \sum_{k \in out(j)} v_{jk}. \tag{34}$$

The idea of the finite-volumes is to construct an algebraic system of equation to express the unknowns $c_j^n \approx c(x_j, t^n)$. The initial values are given by c_j^0. The expression of the interpolation schemes can be given naturally in two ways: the first possibility is given with the primary mesh of the finite-elements

$$c^n = \sum_{j=1}^{I} c_j^n \phi_j(x) \tag{35}$$

where ϕ_j are the standard globally-finite element basis functions (Frolkovič and Geiser 2003). The second possibility is given with the dual mesh of the finite volumes with,

$$\hat{c}^n = \sum_{j=1}^{I} c_j^n \varphi_j(x) \tag{36}$$

where φ_j are piecewise constant discontinuous functions defined by $\varphi_j(x) = 1$ for $x \in \Omega_j$ and $\varphi_j(x) = 0$ otherwise.

4.2 Discretization of the advection equation

If no reactions are considered in (12), the remaining advection equation takes the following form:

$$\partial_t c + \nabla \cdot (\boldsymbol{v} c) = 0 \,. \tag{37}$$

The initial conditions are given by (12), and $c(t, \gamma)$ is explicitly given for $t > 0$ at the inflow boundary $\gamma \in \partial^{in} \Omega$ by (12).

The exact solution of (37) can be directly defined by use of the so-called *forward tracking* form of characteristic curves. If the solution of (37) is known at some time point $t_0 \geq 0$ and some point $y \in \Omega \cup \partial^{in} \Omega$, then u remains constant for $t \geq t_0$ along the characteristic curve $X = X(t)$, i.e. $u(t, X(t)) = u(t_0, y)$ and

$$X(t) = X(t; t_0, y) = y + \int_{t_0}^{t} \boldsymbol{v}(X(s)) \, ds \,. \tag{38}$$

The characteristic curve $X(t)$ starts at the time $t = t_0$ in the point y, i.e. $X(t_0; t_0, y) = y$, and it is tracked forward in time for $t > t_0$. Of course, we can obtain that $X(t) \notin \Omega$, i.e. the characteristic curve can leave the domain Ω through $\partial^{out} \Omega$.

Consequently, we have that $c(t, X(t; t_0, y)) = U(t_0, y)$, where the function $U(0, y)$ is given for $t_0 = 0$ and $y \in \Omega$ by initial conditions (12) and for $t_0 > 0$ and $y \in \partial^{in} \Omega$ by the inflow boundary conditions (12).

The solution $c(t, x)$ of (37) can also be expressed in a backward tracking form, which is more suitable for a direct formulation of the discretization schemes. Concretely, for any characteristic curve $X = X(t) = X(t; s, Y)$, that is defined in a forward manner, i.e. $X(s; s, Y) = Y$ and $t \geq s$, we obtain the curve $Y = Y(s) = Y(s; t, x)$ that is defined in a backward manner, i.e. $Y(t; t, X) = X$ and $s \leq t$. If we express Y as function of t_0 for $t_0 \leq t$, we obtain from (38):

$$Y(t_0) = Y(t_0; t, x) = x - \int_{t_0}^{t} \boldsymbol{v}(X(s)) \, ds \,, \tag{39}$$

12

and we have $c(t, x) = c(t_0, Y(t_0))$.

To simplify our treatment of inflow boundary conditions, we suppose that $U(t, \gamma) = U^{n+1/2} \equiv const$ for $\gamma \in \partial^{in}\Omega$ and $t \in [t^n, t^{n+1})$. Moreover, we define formally for any $\gamma \in \partial^{in}\Omega$ and $t_0 \in [t^n, t^{n+1}]$ that $Y(s; t_0, \gamma) \equiv Y(t_0; t_0, \gamma)$ for $t^n \le s \le t_0$.

In (Frolkovič 2002a), the so-called *flux-based (modified) method of characteristics* was described. This method can be deemed to be an extension of the standard finite volume methods (FVMs)). The standard FVM for differential equations (37) takes the form:

$$|\Omega_j| \, c_j^{n+1} = |\Omega_j| \, c_j^n - \sum_k \int_{t^n}^{t^{n+1}} \int_{\Gamma_{jk}} \boldsymbol{n}_j(\gamma) \cdot \boldsymbol{v}(\gamma) \, c(t, \gamma) \, d\gamma dt \ , \tag{40}$$

The idea of a flux-based method of characteristics is to apply the substitution $c(t, \gamma) = c(t^n, Y(t^n; t, \gamma))$ on (40).

In particular, for the integration variable $t \in (t^n, t^{n+1})$ and for each point $\gamma \in \partial^{out}\Omega_j$, the characteristic curves $Y(s)$ are tracked backward, starting in γ at $s = t$ and ending in $s = t^n$. We must reach a point $Y = Y(t^n)$, such that $Y \in \partial^{in}\Omega$ or $Y \in \Omega$. In the first case, $c(t^n, Y)$ is given by the inflow concentration $U(t^n, Y) = U^n$, in the latter by $c(t^n, Y)$.

The integral on the right-hand side of (40) can be solved exactly for the one-dimensional case with general initial and boundary conditions (Roach 1992). For the general 2D or 3D case, a numerical approximation of $c(t_0, Y(t_0))$, respectively of $Y(t_0)$, will be used (Leveque 2002).

4.3 Discretization method for the convection-reaction equation based on embedded one-dimensional analytical solutions

We apply Godunov's method for the discretization method, cf. (Leveque 2002), and extend the formulation with analytical solution of convection-reaction equations. We reduce the multi-dimensional equation to one-dimensional equations and solve each equation exactly. The one-dimensional solution is multiplied by the underlying volume and we get the mass-formulation. The one-dimensional mass is embedded into the multi-dimensional mass-formulation and we obtain the discretization of the multi-dimensional equation.

13

The algorithm is given in the following manner

$$\partial_t\, c_l + \nabla \cdot \mathbf{v}_l\, c_l = -\lambda_l\, c_l + \lambda_{l-1}\, c_{l-1},$$

with $l = 1, \ldots, m$.

The velocity vector $\mathbf{v}$ is divided by R_l. The initial conditions are given by $c_1^0 = c_1(x,0)$, or $c_l^0 = 0$ for $l = 2, \ldots, m$ and the boundary conditions are trivial $c_l = 0$ for $l = 1, \ldots, m$.

We first calculate the maximal time-step for cell j and concentration i with the use of the total outflow fluxes

$$\tau_{i,j} = \frac{V_j\, R_i}{\nu_j} \,, \quad \nu_j = \sum_{k \in out(j)} v_{jk} \,.$$

We get the restricted time-step with the local time-steps of cells and their components

$$\tau^n \leq \min_{\substack{i=1,\ldots,m \\ j=1,\ldots,I}} \tau_{i,j} \,.$$

The velocity of the discrete equation is given by

$$v_{i,j} = \frac{1}{\tau_{i,j}} \,.$$

We calculate the analytical solution of the mass, cf. (Geiser 2003) and we get

$$m_{i,jk,out}^n = m_{i,out}(a, b, \tau^n, v_{1,j}, \ldots, v_{i,j}, R_1, \ldots, R_i, \lambda_1, \ldots, \lambda_i) \,,$$

$$m_{i,j,rest}^n = m_{i,j}^n\, f(\tau^n, v_{1,j}, \ldots, v_{i,j}, R_1, \ldots, R_i, \lambda_1, \ldots, \lambda_i) \,,$$

where $a = V_j R_i(c_{i,jk}^n - c_{i,jk'}^n)$, $b = V_j R_i c_{i,jk'}^n$ and $m_{i,j}^n = V_j R_i c_{i,j}^n$. Further $c_{i,jk'}^n$ is the concentration at the inflow- and $c_{i,jk}^n$ is the concentration at the outflow-boundary of the cell j.

The discretization with the embedded analytical mass is calculated by

$$m_{i,j}^{n+1} - m_{i,rest}^n = - \sum_{k \in out(j)} \frac{v_{jk}}{\nu_j} m_{i,jk,out} + \sum_{l \in in(j)} \frac{v_{lj}}{\nu_l} m_{i,lj,out} \ ,$$

where $\frac{v_{jk}}{\nu_j}$ is the re-transformation for the total mass $m_{i,jk,out}$ in the partial mass $m_{i,jk}$. In the next time-step the mass is given as $m_{i,j}^{n+1} = V_j \ c_{i,j}^{n+1}$ and in the old time-step it is the rest mass for the concentration i. The proof is provided in (Geiser 2003). In the next section we derive an analytical solution for the benchmark problem, cf. (Higashi and Pigford 1980), (Jury and Roth 1990).

4.4 Discretization of the reaction-equation

The reaction-equation is an ordinary-differential equation is given as follows:

$$\partial_t R_i c_i = -\lambda_i R_i c_i + \lambda_{i-1} R_{i-1} c_{i-1} \ , \tag{41}$$

where $i = 1, \dots, m$ and we denote $\lambda_0 = 0$. The decay-factors are $\lambda_i \geq 0.0$ and the retardation-factors are $R_i > 0.0$. The initial-conditions are $c_1(x, t^0) = c_{01}$ and $c_i(x, t^0) = 0$ with $i = 2, \dots, m$.

We can derive the solutions for these equations, cf. (Bateman 1910), as

$$c_i = c_{01} \frac{R_1}{R_i} \Lambda_i \sum_{j=1}^{i} \Lambda_{j,i} \exp(-\lambda_j \ t) \ , \tag{42}$$

where $i = 1, \dots, m$. The solutions are defined for the case $\lambda_j \neq \lambda_k$ with $j \neq k$ and $j, k \in 1, \dots, M$.

The factors Λ_i and $\Lambda_{j,i}$ are given as

$$\Lambda_i = \prod_{j=1}^{i-1} \lambda_j \ , \quad \Lambda_{j,i} = \prod_{\substack{j=1 \\ j \neq k}}^{i} \frac{1}{\lambda_k - \lambda_j} \ . \tag{43}$$

For wise equal reaction-factors we have derived the solution (Geiser 2003).

In the next subsection we introduce the discretization of the diffusion-dispersion-equation.

4.5 Discretization of the source-terms

The source terms are part of the convection-diffusion equations and are given as follows:

$$\partial_t c_i(x,t) - \mathbf{v} \cdot \nabla c_i + \nabla D \nabla c_i = q_i(x,t) \ , \tag{44}$$

where $i = 1, \ldots, m$, $\mathbf{v}$ is the velocity, D is the diffusion tensor and $q_i(x,t)$ are the source functions, which can be point wise, linear in the domain.

The point wise sources are given as :

$$q_i(t) = \left\{ \begin{array}{ll} \frac{q_{s,i}}{T} & t \leq T, \\ \\ 0 & t > T, \end{array} \right. \quad , \text{with} \int_T q_i(t)dt = q_{s,i}, \tag{45}$$

where $q_{s,i}$ is the concentration of species i at source point $x_{source,i} \in \Omega$ over the whole time-interval.

The line and area sources are given as :

$$q_i(x,t) = \left\{ \begin{array}{ll} \frac{q_{s,i}}{T|\Omega_{source,i}|}, & t \leq T \text{ and } x \in \Omega_{source,i}, \\ \\ 0, & t > T, \end{array} \right. ,\tag{46}$$

$$\text{with} \int_{\Omega_{source,i}} \int_T q_i(x,t)dtdx = q_{s,i},$$

16

where $q_{s,i}$ is the source concentration of species i at the line or area of the source over the whole time-interval.

For the finite-volume discretization we have to compute :

$$\int_{\Omega_{source,i,j}} q_i(x,t) \, dx = \int_{\Gamma_{source,i,j}} \mathbf{n} \cdot (\mathbf{v} c_i - D\nabla c_i) \, d\gamma \, , \tag{47}$$

where $\Gamma_{source,i,j}$ is the boundary of the finite-volume cell $\Omega_{source,i,j}$ which is a source area. We have $\cup_j \Omega_{source,i,j} = \Omega_{source,i}$ where $j \in I_{source}$, where I_{source} is the set of the finite-volume cells that includes the area of the source.

The right-hand side of (47) is also called the flux of the sources (Frolkovič 2002b).

In the next subsection we introduce the discretization of the diffusion-dispersion-equation.

4.6 Discretization of the diffusion-dispersion-equation

We discretize the diffusion-dispersion-equation with implicit time-discretization and the finite-volume method for the following equation

$$\partial_t R \, c - \nabla \cdot (D\nabla c) = 0 \, , \tag{48}$$

where $c = c(x,t)$ with $x \in \Omega$ and $t \geq 0$. The diffusions-dispersions-tensor $D = D(x,\mathbf{v})$ is given by the Scheidegger-approach (Scheidegger 1961). The velocity is given as $\mathbf{v}$. The retardation-factor is $R > 0.0$.

The boundary-values are denoted by $\mathbf{n} \cdot D \, \nabla c(x,t) = 0$, where $x \in \Gamma$ is the boundary $\Gamma = \partial\Omega$, (Frolkovič 2002a). The initial conditions are given by $c(x,0) = c_0(x)$.

We integrate the equation (48) over space and time and derive

$$\int_{\Omega_j} \int_{t^n}^{t^{n+1}} \partial_t R(c) \, dt \, dx = \int_{\Omega_j} \int_{t^n}^{t^{n+1}} \nabla \cdot (D\nabla c) \, dt \, dx \, . \tag{49}$$

17

The time-integration is done by the backward-Euler method and the diffusion-dispersion term is lumped, (Geiser 2003)

$$\int_{\Omega_j} (R(c^{n+1}) - R(c^n))\, dx = \tau^n \int_{\Omega_j} \nabla \cdot (D\nabla c^{n+1})\, dx \, , \tag{50}$$

The equation (50) is discretized over the space with Green's-formula.

$$\int_{\Omega_j} (R(c^{n+1}) - R(c^n))\, dx = \tau^n \int_{\Gamma_j} D\, \mathbf{n} \cdot \nabla c^{n+1}\, d\gamma \, , \tag{51}$$

where Γ_j is the boundary of the finite-volume cell Ω_j. We use the approximation in space (Geiser 2003).

The spatial-integration for (51) is done by the mid-point rule over the finite boundaries and is given as

$$V_j R(c_j^{n+1}) - V_j R(c_j^n) = \tau^n \sum_{e \in \Lambda_j} \sum_{k \in \Lambda_j^e} |\Gamma_{jk}^e| \mathbf{n}_{jk}^e \cdot D_{jk}^e \nabla c_{jk}^{e,n+1} \, , \tag{52}$$

where $|\Gamma_{jk}^e|$ is the length of the boundary-element Γ_{jk}^e. The gradients are calculated with the piecewise finite-element-function ϕ_l, cf. (35) and we obtain

$$\nabla c_{jk}^{e,n+1} = \sum_{l \in \Lambda^e} c_l^{n+1} \nabla \phi_l(\mathbf{x}_{jk}^e) \, . \tag{53}$$

With the difference-notation we get for the neighbor-point j and l (Frolkovič and De Schepper 2001) and get the discretized equation

$$V_j R(c_j^{n+1}) - V_j R(c_j^n) = \tag{54}$$
$$\tau^n \sum_{e \in \Lambda_j} \sum_{l \in \Lambda^e \setminus \{j\}} \left(\sum_{k \in \Lambda_j^e} |\Gamma_{jk}^e| \mathbf{n}_{jk}^e \cdot D_{jk}^e \nabla \phi_l(\mathbf{x}_{jk}^e) \right) (c_j^{n+1} - c_l^{n+1}) \, ,$$

18

where $j = 1, \ldots, m$.

5 REGRESSION AND APPROXIMATION OF THE PARAMETERS

We apply regression analysis to includes the techniques for modeling and analyzing several variables.

We have the dependent variables (physical parameters) and one and more independent variables (mathematical parameters).

Therefore we understand how the typical value of the dependent variable changes when any one of the independent variables is varied, while the other independent variables are held fixed. It is also of interest to characterize the variation of the dependent variable around the regression function, which can be described by a probability distribution.

The regression models involve the following variables:

- The unknown parameters denoted as β; this may be a scalar or a vector of length k.

- The independent variables, X.

- The dependent variable, Y.

A regression model relates Y to a function of X and β.

$$Y \approx f(\mathbf{X}, \boldsymbol{\beta}). \tag{55}$$

The approximation is usually formalized as $E(Y|X) = f(X,)$. To carry out regression analysis, the form of the function f must be specified.

We concentrate on linear regression:

1.) We exactly $N = k$ data points are observed, and the function f is linear, so the equation $Y = f(X,)$ can be solved exactly rather than approximately. This reduces to solving a set of N

19

equations with N unknowns (the elements of β), which has a unique solution as long as the X are linearly independent.

2.) We have $N > k$ data points. In this case, there is enough information in the data to estimate a unique value for β that best fits the data in some sense, and the regression model when applied to the data can be viewed as an overdetermined system in β.

Method:

Finding a solution for unknown parameters β that will, for example, minimize the distance between the measured and predicted values of the dependent variable Y (also known as method of least squares).

Means we have at least to compute the function F:

$$\hat{Y} = XF, \tag{56}$$

$$Y_{reg} = X_{new}F, \tag{57}$$

$$Y - \hat{Y} = Err, \tag{58}$$

where Y is the exact value and $\hat{Y}$ the approximated values, F is the regression function.

Algorithm:

We apply the multi-physics equation with mass transport with a system of convection-diffusion-reaction equations with embedded sorption equations.

For all the experiments we approximate the physical experiment with a mathematical experiment and obtain parameter for the simulation models. Later we apply by regression new parameters in the physical experiment to have some tendencies, see (Geiser and Arab 2010). A superposition of the single regression functions is applied to derive the new regression functions.

In the next section, we discuss the numerical experiments.

6 NUMERICAL EXPERIMENTS

In the following, we present the numerical experiments, which are compared with physical experiments. We apply the physical results of the deposition rates and approximate to our model equations with respect to the reaction and retardation parameters.

Based on this parameters, we could approximate to different parameters in the simulations and achieve numerical deposition rates, which could be used for a preview of physical experiments.

For all the experiments we have the following parameters of the model, the discretization and solver methods.

We apply interpolation and regression methods to couple the physical parameters to the mathematical parameters, see Figure 4 and Table 1.
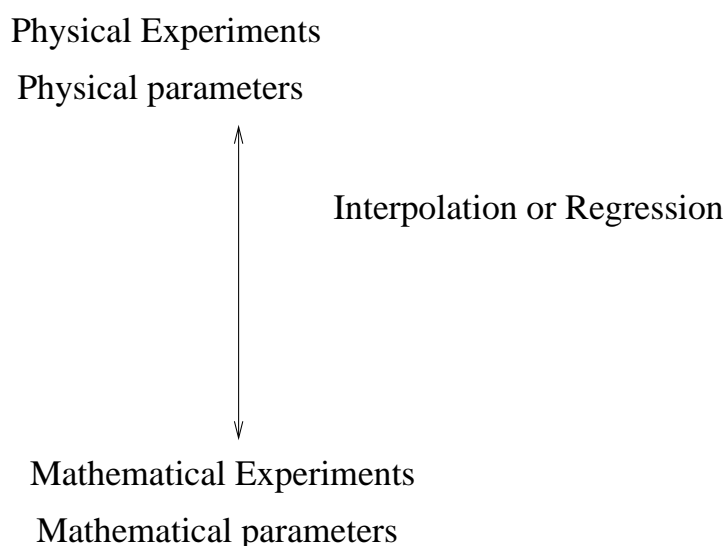
<div align="center">

Physical Experiments

Physical parameters

↑

Interpolation or Regression

↓

Mathematical Experiments

Mathematical parameters

</div>

Figure 4: Coupling of physical and mathematical parameter space.

Physical parameter	Mathematical parameter
Temperature,pressure,power	velocity, Diffusion,Reaction
T , p , W	V , D , λ

Table 1: Physical and mathematical parameters.

In the following Figure 5 the underlying geometry of the apparatus is given. The inflow of the precursor gases are at left and right the top of the apparatus, while the outflows are at the left

and right bottom. The measure point $(130, 70)$ is in the middle of the deposition area and the deposition rates could be measured.
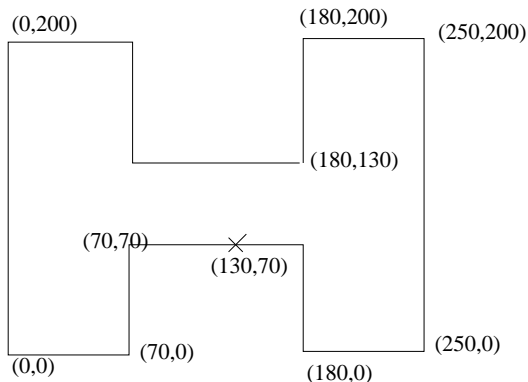

Figure 5: The geometry of the apparatus with the measure points.

6.1 Parameters of the model equations

In the following all parameters of the model equations (12) are given in Table 3.

density	$\rho = 1.0$
mobile porosity	$\phi = 0.333$
immobile porosity	0.333
Diffusion	$D = 0.0$
longitudinal Dispersion	$\alpha_L = 0.0$
transversal Dispersion	$\alpha_T = 0.00$
Retardation factor	$R = 10.0e - 4$ (Henry rate).
Velocity field	$\boldsymbol{v} = (0.0, -4.0\ 10^{-8})^t$.
Decay rate of the species of 1st EX	$\lambda_{AB} = 1\ 10^{-68}$.
Decay rate of the species of 2nd EX	$\lambda_{AB} = 2\ 10^{-8}, \lambda_{BNN} = 1\ 10^{-68}$.
Decay rate of the species of 3rd EX	$\lambda_{AB} = 0.25\ 10^{-8}, \lambda_{CB} = 0.5\ 10^{-8}$.
Geometry (2d domain)	$\Omega = [0, 100] \times [0, 100]$.
Boundary	Neumann boundary at
	top, left and right boundaries.
	Outflow boundary
	at the bottom boundary

Table 2: Model-Parameters.

The discretization and solver method are given as:

For the spatial discretization method, we apply Finite volume methods of 2nd order, with the following parameters in Table 3.

22

spatial step size	$\Delta x_{min} = 1.56, \Delta x_{max} = 2.21$
refined levels	6
Limiter	Slope limiter
Test functions	linear test function
	reconstructed with neighbor gradients

Table 3: Spatial discretization parameters.

For the time discretization method, we apply Crank-Nicolson method (2nd order), with the following parameters in Table 4.

Initial time-step	$\Delta t_{init} = 5 \; 10^7$
controlled time-step	$\Delta t_{max} = 1.298 \; 10^7, \Delta t_{min} = 1.158 \; 10^7$
Number of time-steps	$100, 80, 30, 25$
Time-step control	time steps are controlled with
	the Courant-Number $\mathrm{CFL}_{max} = 1$

Table 4: Time discretization parameters.

For the discretised equations are solved with the following methods, see the description in Table 5.

Solver	BiCGstab (Bi conjugate gradient method)
Preconditioner	geometric Multi-grid method
Smoother	Gauss-Seidel method as smoothers for
	the Multi-grid method
Basic level	0
Initial grid	Uniform grid with 2 elements
Maximum Level	6
Finest grid	Uniform grid with 8192 elements

Table 5: Solver methods and their parameters.

For the numerical experiments, we discuss the approximation to the SiC and TiC experiments.

The underlying software tool is $r3t$, which was developed to solve discretised partial differential equations. We use the tool to solve transport-reaction equations, see (Fein 2004).

6.2   Test Experiment with SiC deposition (Near Field)

For the SiC, we obtain a different setup for the physical experiment, including the Bias voltage of the electric field, which is simulated as retardation to the species.

23

For simplification of the reactive process, we consider the last kinetic process, given as:

$$2SiC + 4H \rightarrow_\lambda SiC + CH_4 + Si, \tag{59}$$

Here we have the physical experiments and approximate to the temperature parameters of $T = 400, 600, 800$. For the physical experiment we have the following parameters:

W	T	P_{mbar}	R_{Si}	R_C	Physical ratio(Si:C)	Numerical ratio(Si:C)
100	700	9.7e-02	4e-04	2e-04	0.569	0.568
300	700	9.7e-02	2.3e-04	2e-04	0.744	0.740
900	700	9.7e-02	1.35e-04	2e-04	0.919	0.9
100	400	1e-01	2e-04	0.7e-04	0.617	0.6103
500	400	1e-01	2e-04	1.6e-04	0.757	0.745
500	400	1e-01	2e-04	1.3e-04	0.704	0.691
900	400	1e-01	2e-04	3.48e-04	1.010	1.017
900	400	1e-01	2e-04	3.4e-04	1.0	1.0
100	400	4.5e-02	4.7e-04	0.1e-04	0.342	0.342

Table 6: Approximated Deposition rates and comparison to physical experiments.

In the following numerical experiment, we apply the deposition area (near field), see Figure 4.

Here we assume to have a constant velocity field and start with the species SiC and H, which are given as point and line sources, see Table 8.

81 point sources of SiC at the position	$X = 10, 11, 12, \ldots, 90, Y = 20$
Line source of H at the position	$x \in [5, 95], y \in [20, 25]$
Amount of the permanent source concentration	$SiC_{source} = 0.4, 0.7, 0.8, 0.85, 0.84, 0.82, 0.8$,0.6,0.4,0.2,0.0., $H_{source} = 0.12$
Number of time steps	200

Table 7: Parameter of the source concentration.

We take here the concentration of SiC as a point sources, and the concentration of H is a line source.

In Figure 6, we present the concentration after 100 and 200 time-steps.
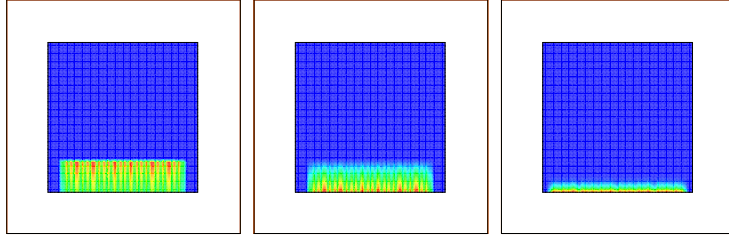
Figure 6: Experiment with moving point sources, where SiC experiment after 200 time-steps.
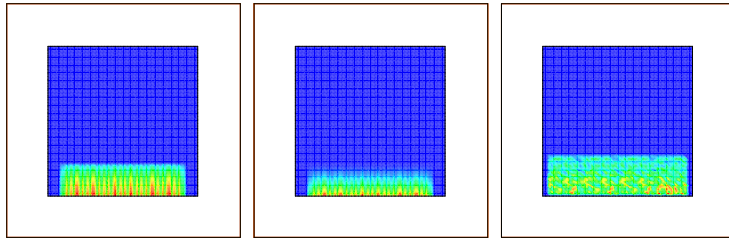

Figure 7: Experiment with moving point sources, where SiC experiment after 200 time-steps.

In Figure 8, we show the deposition rates of the 81 point sources experiment.
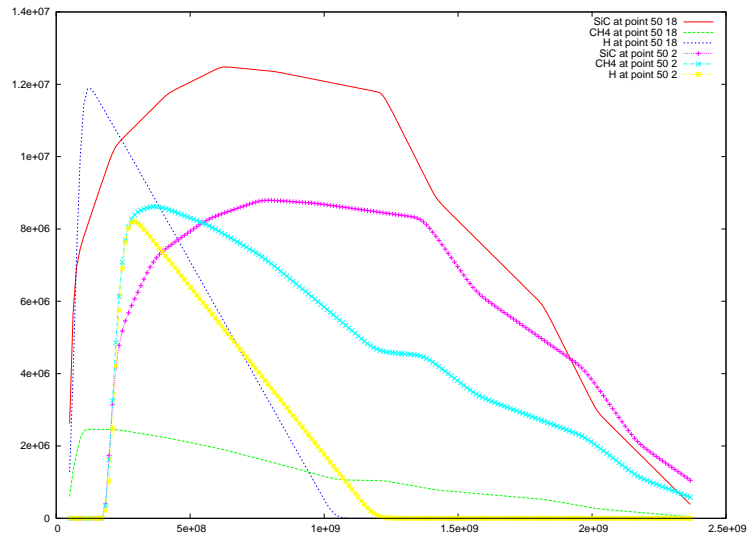

Figure 8: Deposition rates in case of 81 point sources experiment.

Remark 2 *The numerical experiments can be fitted in the near field to the physical experiments. In different situations, the best deposition result is obtained with at least homogeneous*

25

RATE
$C_{source,max} : SiC_{target,max}$
$8.7.10^6 : 8.7.10^6 = 1.$

Table 8: Rate of the concentration.

concentrations below the deposition area. The near field simulations obtain an optimum at low temperature $400[^oC]$ and high plasma power about $900[W]$. Such results are also obtained in our physical studies, see (Geiser and Arab 2010).

6.3 Test Experiment with TiC deposition (Fare field)

For the TiC, we obtain a different setup for the physical experiment, including the Bias voltage of the electric field, which is simulated as retardation to the species. In the following numerical experiment, we apply the deposition area (fare field), see Figure 4. Such a contrast to the near field allows to specify the situation in the whole apparatus.

For the physical experiment we have the following parameters:

Pressure in the chamber	$p = 9.810^{-2} - 2[mbar]$
Precursor temperature	$T_{precursor} = 71.5[^0C]$
Velocity (argon gas)	$v = 30.0[cm^3/min]$
Inflow velocity of the	
precursor gas	$v_{inflow} = 0.60[cm^3/min]$

Table 9: Physical parameters.

Based on the approximation scheme, we apply the simulation with respect to derive the mathematical parameters.

For different physical situations, we could achieve the following mathematical parameters, see Table 10.

In the following Figure 9 and 10, we present an example of the concentration of two inflow sources $x_{Ti}, y_{Ti} = (35, 190)$ and $x_{Ti}, y_{Ti} = (215, 190)$. The velocity is given perpendicular to the apparatus.

Power [W]	Bias [V]	R_C at material 1	R_{Ti} at material 2	Ratio(C:Ti) (numerical)
300	0	$0.1\ 10^{-4}$	$20\ 10^{-4}$	$5.5 : 1.5 = 3.6$
600	0	$1.0\ 10^{-4}$	$20\ 10^{-4}$	$4.4 : 1.5 = 2.93$
900	0	$1.5\ 10^{-4}$	$20\ 10^{-4}$	$3.8 : 1.5 = 2.53$
300	-10	$2.8\ 10^{-4}$	$20\ 10^{-4}$	$3.1 : 1.5 = 2.066$
600	-10	$1.0\ 10^{-15}$	$20\ 10^{-4}$	$5.7 : 1.5 = 3.8$
900	-10	$1.0\ 10^{-15}$	$60\ 10^{-4}$	$5.7 : 05 = 11.4$

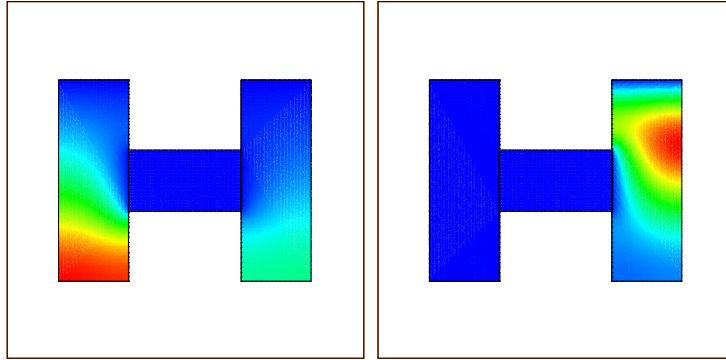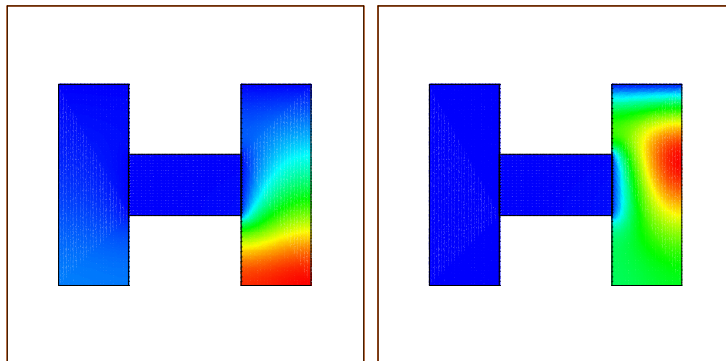Table 10: Computed and experimental fitted parameters with UG simulations.

Figure 9: Two inflow sources $x_{Ti}, y_{Ti} = (35, 190)$ and $x_{Ti}, y_{Ti} = (215, 190)$ with perpendicular velocity and 100 time-steps with ratio between C and Ti equal to 3.6.

Figure 10: Two inflow sources $x_{Ti}, y_{Ti} = (35, 190)$ and $x_{Ti}, y_{Ti} = (215, 190)$ with perpendicular velocity and 150 time-steps with ratio between C and Ti equal to 3.6.

In Figure 11, we show the deposition rates of two inflow sources $x_{Ti}, y_{Ti} = (35, 190)$ and $x_{Ti}, y_{Ti} = (215, 190)$ with perpendicular velocity and after 150 time-steps.
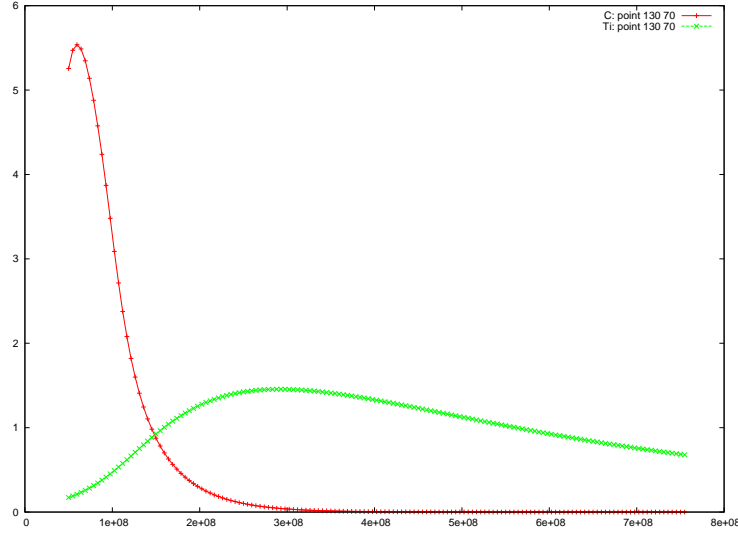
27

Figure 11: Deposition rates in case of two point sources,x= 35,215. y=190.with perpendicular velocity and 150 time-steps with ratio between C and Ti equal to 3.6.

Remark 3 *The numerical experiments can also be fitted in the fare field to the physical experiments. By the way the situations are more delicate. The best deposition result is obtained with at least different flow regimes in the left and right inflow sources, means the mixture in the deposition area is optimal. The fare field simulations obtain an optimum at lower temperature $300[^oC]$ and a high bias voltage about $-10[V]$. Such prognostic results are also obtained in our physical studies.*

7   CONCLUSION

We have presented a model for the chemical vapor deposition processes. The approximations are done to a realistic apparatus with transport-reaction. The equations are discretized by the finite volume method and the complex material functions are embedded in this method. The approximation methods to the numerical parameters are presented. We present numerical results for the stoichiometry for SiC and TiC depositions. Near and fare field simulations can derive an optimal parameter setting and prognostic results to future experiments. Such simulations help to reduce physical experiments and gave tendencies to future expensive physical experiments. In our future work, we concentrate on further implementations and numerical methods

28

for a full growth model.

REFERENCES

Bateman H (1910). The solution of a system of differential equations occurring in the theory of radioactive transformations. *Proc. Cambridge Philos. Soc. 15*(5), pp. 423–427.

Fein E (2004). Software package r3t - model for transport and retention in porous media. Technical Report GRS-192, Gesellschaft für Anlagen- und Reaktorsicherheit (GRS) mbH.

Frolkovič P (2002a). Flux-based method of characteristics for contaminant transport in flowing groundwater. *Computing and Visualization in Science 5*(2), pp. 73–83.

Frolkovič P (2002b). Flux-based methods of characteristics for transport problems in groundwater flows induced by sources and sinks. *Computational Methods in Water Resources (S.M. Hassanizadeh et al.)Volume II., Elsevier, Amsterdam, Boston, Heidelberg,.*

Frolkovič P and De Schepper H (2001). Numerical modelling of convection dominated transport coupled with density driven flow in porous media. *Advances in Water Resources 24*, pp. 63–72.

Frolkovič P and Geiser J (2003). Discretization methods with discrete minimum and maximum property for convection dominated transport in porous media. *I. Dimov, I. Lirkov, S. Margenov and Z. Zlatev (eds.), Numerical Methods and Applications, 5th International Conference, NMA 2002*, Borovets, Bulgaria. Berlin, Heidelberg, pp. 446–453.

Geiser, J Buck V and Arab M (2010). Model of pe-cvd apparatus: Verification and simulations. *Mathematical Problems in Engineering, Hindawi Publishing Corp., New York, USA. accepted 2010.*

Geiser J (2001). Numerical simulation of a model for transport and reaction of radionuclides. *Proceedings of the Large Scale Scientific Computations of Engineering and Environmental Problems*, Sozopol, Bulgaria.

Geiser J (2003). *Gekoppelte Diskretisierungsverfahren für Systeme von Konvektions-Dispersions-Diffusions-Reaktionsgleichungen.* Ph. D. thesis, Universität Heidelberg.

Geiser J and Arab M (2008). Modelling for chemical vapor deposition: Meso- and microscale model. *International Journal of Applied Mathematics and Mechanics (IJAMM) accepted 2008.*

Gobbert MK and Ringhofer CA (1998). An asymptotic analysis for a model of chemical vapor deposition on a microstructured surface. *SIAM Journal on Applied Mathematics 58*(1), pp. 737–752.

Higashi K and Pigford ThH (1980). Analytical models for migration of radionuclides in geologic sorbing media. *Journal of Nuclear Science and Technology 17(9).*

Jury WA and Roth K (1990). *Transfer Functions and Solute Movement through Soil.* Basel, Boston, Berlin: Bikhäuser Verlag.

Kadetov VA (2004). *Diagnostics and modeling of an inductively coupled radio frequency discharge in hydrogen.* Ph. D. thesis, Ruhr Universität Bochum.

Leveque RJ (2002). *Finite Volume Methods for Hyperbolic Problems.* Cambridge Texts in Applied Mathematics, Cambridge, UK.

Ohring M (2002). *Materials Science of Thin Films.* Academic Press, San Diego, New York, Boston, London. Second Edition.

Roach PJ (1992). A flux-based modified method of characteristics. *Int. J. Numer. Methods Fluids 12.*

Scheidegger AE (1961). General theory of dispersion in porous media. *Journal of Geophys. Res. 66*, pp. 32–73.

Senega TK and Brinkmann RP (2006). A multi-component transport model for non-equilibrium low-temperature low-pressure plasmas. *J. Phys. D: Appl. Phys. 39*(1), pp. 1606–1618.